physica status solidi a
www.pss-a.com

Recent Progress in Understanding the Properties of the Amorphous Silicon/Crystalline Silicon Interface

Jean-Paul Kleider, José Alvarez, Rudolf Brüggemann, and Marie-Estelle Gueunier-Farret*

The authors review experimental and modeling approaches developed at GeePs to have a better knowledge and understanding of the interface between hydrogenated amorphous silicon (a-Si:H) and crystalline silicon (c-Si) in heterojunction solar cells. The authors emphasize the existence of a strong inversion layer at the c-Si surface for both (n) a-Si:H/(p) c-Si and (p) a-Si:H/(n) c-Si heterojunctions. Conductive probe atomic force microscopy reveals the existence of a conductive channel at the c-Si surface. The analysis of complementary lateral planar conductance and capacitance measurements allows for a better description of the band diagram in both types of heterojunctions especially through the determination of band offset values. Furthermore, the passivation properties of the (i) a-Si:H buffer layer are studied by modeling the volume defects in a-Si:H with the defect-pool model. In particular, the DOS in the very thin (i) a-Si:H layers is much larger than in bulk (i) a-Si:H because the Fermi level position favors defect creation. Surface defects in c-Si at the a-Si:H/c-Si interface are then quantified and the general trends of effective lifetime measurements with the (i) a-Si:H layer thickness can be explained, notably the increase of the effective lifetime in c-Si with increasing the (i) a-Si:H buffer thickness.

1. Introduction

While crystalline silicon (c-Si) has been studied and developed since the 1950s for both microelectronics and photovoltaics (PV),[1] studies on hydrogenated amorphous silicon (a-Si:H) have gained momentum in the 1970s.[2,3] With the possibility of fabricating thin-film transistors on large areas, they have led in the 1980s to the development of LCD flat panel display applications.[4] However, as far as PV is concerned and despite substantial improvement in efficiencies and stability of thin film a-Si:H solar cells,[5] this technology only reached a very small part of the PV market that is largely dominated by mono- and multicrystalline Si technologies.[6] The two worlds of amorphous and crystalline matter and their application in PV have gone their own way with their own physics until the Sanyo laboratories took up previous ideas[7] and demonstrated that a-Si:H/c-Si interfaces could replace the traditional diffused junctions in c-Si photovoltaics and lead to very high energy conversion efficiencies.[8] As a matter of fact, the highest efficiency reached so far for a c-Si based solar cell employs an n-type c-Si substrate with bottom electron and hole extracting contacts using (n) a-Si:H and (p) a-Si:H layers, respectively.[9]

Interface recombination is a key issue for these PV applications. It has been recognized that an undoped a-Si:H buffer layer – so called intrinsic, (i) a-Si:H, inserted between the doped crystalline absorber and the doped a-Si:H layer plays a beneficial role, improving the open circuit voltage of silicon heterojunction (Si-HET) cells.[10] This improved passivation is related to a reduction of interface recombination, which has been attributed to a reduction of interface states, sometimes referred as chemical passivation.[11] However, the interface states density could never be measured, and the quality of the device is generally assessed through the open circuit voltage of the cell or the effective lifetime in the c-Si wafer, measured from various techniques like photoluminescence, photoconductivity decay or from other techniques.[12] We here give a summary of our knowledge of the a-Si:H/c-Si interface in terms of device physics. We emphasize the role of strong inversion of the silicon surface in both (p) a-Si:H/(n) c-Si and (n) a-Si:H/(p) c-Si heterojunctions. We review the approaches developed in our laboratory to determine band offsets and analyze interface recombination through measurements from various characterization techniques and modeling based on the defect-pool model in a-Si:H.

2. Determination of Band Diagrams at Silicon Heterojunctions

Band offsets at the a-Si:H/c-Si heterojunctions are fundamental parameters to understand the physics of Si-HET devices and they are necessary input parameters for device simulation. This is why a lot of efforts have been deployed to accurately determine these parameters using various characterization techniques. In

Dr. J.-P. Kleider, Dr. J. Alvarez, Dr. R. Brüggemann,
Dr. M.-E. Gueunier-Farret
GeePs, UMR 8507 CNRS
CentraleSupélec, Univ. Paris-Sud
Université Paris-Saclay
Sorbonne Université
11, rue Joliot-Curie, 91192 Gif-sur-Yvette, France
E-mail: jean-paul.kleider@geeps.centralesupelec.fr

DOI: 10.1002/pssa.201800877

the following, the (n) a-Si:H/(p) c-Si and (p) a-Si:H/(n) c-Si heterojunctions will be denoted N/p and P/n.

The equilibrium band diagrams of the N/p and P/n heterojunctions are shown in **Figure 1** and **Figure 2**, respectively. The total electrostatic potential drop, called built-in or diffusion potential V_d can be separated into the part in a-Si:H, $V_d^{a-Si:H}$, and that in c-Si, V_d^{c-Si}. Due to the large density of states (DOS) at the Fermi level E_F in the bandgap of doped a-Si:H, $V_d^{a-Si:H}$ is much smaller than V_d^{c-Si}. The position of the Fermi level is separated from the majority carrier band by $\delta^{c\text{-}Si}$ in c-Si and $\delta^{a\text{-}Si:H}$ in a-Si:H. The conduction and valence band offsets at the interface are defined as $\Delta E_C = E_C^{a-Si:H} - E_C^{c-Si}$, and $\Delta E_V = E_V^{c-Si} - E_V^{a-Si:H}$.

The c-Si wafers used for solar cell applications have resistivities of the order of 1 Ω cm, corresponding to room temperature values of 0.2–0.25 eV for $\delta^{c\text{-}Si}$. The doped a-Si:H layers have typical values $\delta^{a\text{-}Si:H}$ of 0.2 eV for (n) a-Si:H and 0.35 eV for (p) a-Si:H. The values of $V_d^{a-Si:H}$ and V_d^{c-Si} are typically found around 0.05 and 0.85 V, respectively. In both N/p and P/n heterostructures the Fermi level at the interface is very close to the edge of the minority carrier band of the c-Si wafer: the strong band bending in c-Si is related to a strong inversion layer at the c-Si surface.

We here briefly review how the presence of the strong inversion layers could be evidenced by the results obtained in our group from a set of complementary experimental techniques: lateral conductance, conductive probe atomic force microscopy (CP-AFM) and capacitance measurements. This also led us to estimate the conduction and valence band offsets to about $\Delta E_C = 0.15$ eV and $\Delta E_V = 0.4$ eV for the structures we analyzed. However, it has to be mentioned that the bandgap of a-Si:H depends on deposition conditions. In particular, larger hydrogen content leads to larger bandgap,[13] which in turn leads to larger band offsets.[14]

2.1. Lateral Conductance

Measurements of the lateral conductance have been performed both on (n) a-Si:H/(p) c-Si structures,[15,16] and on (p) a-Si:H/(n) c-Si structures,[17,18] using the schematic principle given in **Figure 3**.

The a-Si:H layer was deposited onto flat c-Si wafers after some cleaning step (HF dip), and in the same run onto glass substrates. While for solar cell applications the thickness of the a-Si:H layer is typically less than 20 nm, thicker layers (up to 200 nm) were also deposited in order to have reliable conductance measurements on glass. Top coplanar electrodes are then deposited onto the a-Si:H surface. It is interesting to have several identical electrodes with various values of the gap, between them, for example, in the range of 0.5–5 mm, in order to check that the contact resistance is negligible compared to the resistance of the a-Si:H/c-Si structure (TLM method). The length, h, and width, w, of the electrodes is not so important, typical widths of a few mm and lengths of 5–20 mm can be used in order to have aspect ratios h/w and h/L of the electrode design significantly larger than one such as to minimize edge effects. From the measurement of the current as a function of bias one can check the linearity and extract the conductance, G. For both N/p and P/n heterojunction structures, the conductance is

Jean-Paul Kleider graduated from the SUPELEC school of engineering in 1984 and obtained his PhD in physics at the University Pierre et Marie Curie in 1987. He has been holding a researcher position at CNRS since 1988. Since 2015, he is leading the department of Physics and Electronics of Materials, Devices, Interfaces and Contacts at GeePs. His main research interests lie in the electrical and optoelectronic characterization of semiconductor materials and in device physics including theoretical analysis and numerical modelling.

Jose Alvarez received the M.S. degree in microelectronics from Denis Diderot University (Paris 7) in 2000, and the Ph.D. degree from UPMC (Paris 6) in 2004. Since October 2005, he has been working as a researcher at GeePs (CNRS UM8507) on optical and electrical characterization and optimization of semiconductor materials and devices. His current fields of interest are linked to the scanning probe microscopy and confocal microscopy (Raman and photoluminescence) characterization techniques applied to material and device fundamental studies and failure analysis.

Rudolf Brüggemann received an MSc from Dundee University in 1987, a Diploma in Physics in 1989 and his PhD degree in 1993, the latter two from the University of Marburg. He worked at the universities in Stuttgart and Oldenburg, receiving his Habilitation degree in 2003. He has been a member of the Group of Electrical Engineering Paris since March 2015. His research interests lie in the optoelectronic characterisation of semiconductors and solar cells by experimental and numerical-modelling techniques.

Marie Gueunier-Farret graduated from the SUPELEC school of engineering in 2000, received her Ph.D. degree in physics from the University Paris-Sud in 2003 and her habilitation (HDR) in 2014. She's been an Associate Professor since 2004 with research responsibilities in the Physics and Electronics of Materials, Devices, Interfaces and Contacts department of GeePs laboratory. Her research interests include the development of theoretical background and experimental set-up of characterization techniques as well as numerical modeling to study materials and devices for photovoltaics.

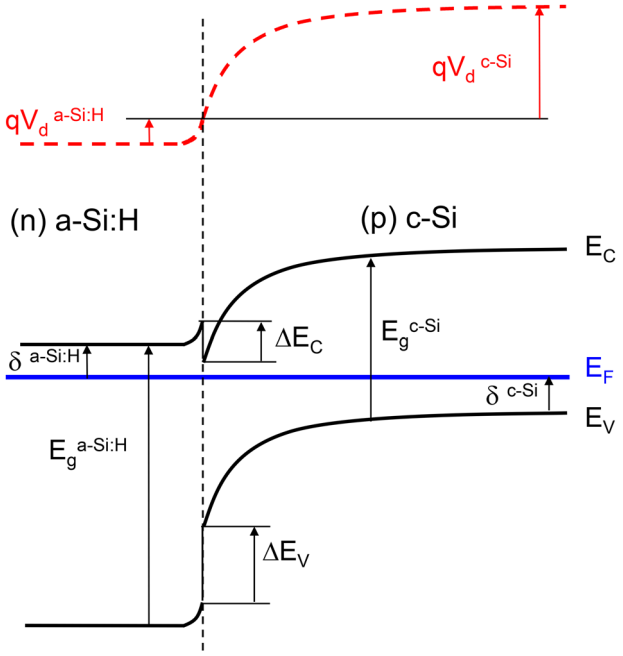

Figure 1. Schematic equilibrium band diagram of the (n) a-Si:H/(p) c-Si heterojunction. The dashed red line indicates the vacuum level and the potential drops in a-Si:H and c-Si, $V_d^{a-Si:H}$ and V_d^{c-Si}, respectively.

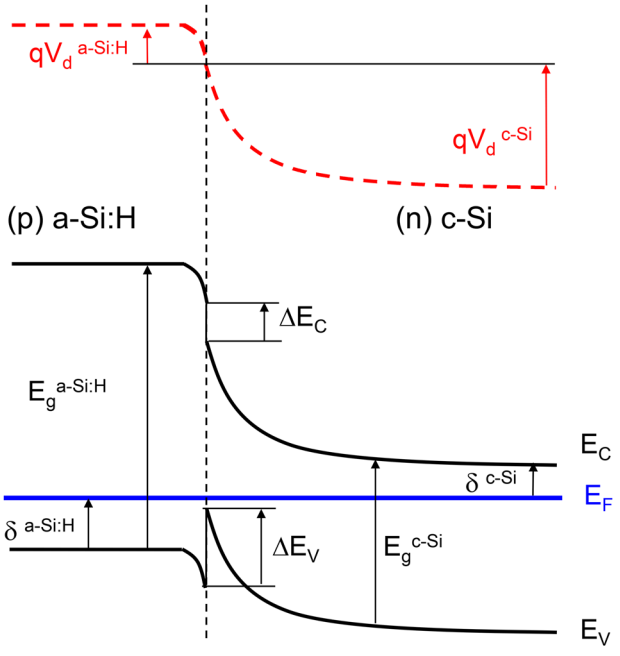

Figure 2. Schematic equilibrium band diagram of the (p) a-Si:H/(n) c-Si heterojunction. The dashed red line indicates the vacuum level and the potential drops in a-Si:H and c-Si, $V_d^{a-Si:H}$ and V_d^{c-Si}, respectively.

several orders of magnitude larger than for the corresponding a-Si:H layers deposited on glass (**Figure 4**).

We considered three possible paths for the current flow between two coplanar top electrodes, as indicated in **Figure 5**. The first path is simply through the a-Si:H layer. However, the much lower conductance observed when a-Si:H is deposited on glass proves that it gives a negligible contribution in the heterostructures. Also, the conductance of the samples on glass was found to scale with the a-Si:H thickness, while the conductance of the samples on c-Si was almost independent of the a-Si:H thickness. It might be argued that the structure of a-Si:H might be different when deposited on glass or on c-Si. However, this could hardly explain the observed orders of magnitude changes. In addition, transmission electron microscopy (TEM) clearly shows that the deposited silicon layer was amorphous.[19] Also, we changed the deposition conditions of a-Si:H, turning to a polymorphous type material[20] for the first deposited nanometers without strong change in the measured heterostructure conductance.[15] The second path is through the c-Si wafer. However, the current starting from one top electrode has to go through the thickness of the a-Si:H layer, cross the N/p heterojunction, move in the c-Si toward the second electrode, and then cross the p/N heterojunction and the a-Si:H layer in order to reach the second top electrode. Crossing both the N/p and p/N heterojunctions means that, whatever the bias applied between the two electrodes, the current is then limited by one of the heterojunctions that is reverse biased. Therefore, this path should also bring a negligible contribution to the overall planar heterostructure conductance. One might argue that the heterojunction could be locally shunted, so that the reverse bias would not induce strong limitation of the current. To prove that this is not the case, we dry etched the a-Si:H layer using the metal electrodes as a mask. Figure 5 compares the conductance for the two structures. The conductance after etching was found orders of magnitude lower and the corresponding activation energy E_a becomes much larger (0.72 eV), as expected from the current in a reverse biased heterojunction. Finally, the only remaining explanation for the large planar heterostructure conductance is a high interface conductance G_{int} that is due to a strongly inverted layer at the c-Si surface, as can be seen in Figure 1 and 2.

For the N/p heterostructure, the band bending forms an electron channel at the c-Si surface, 2DEG (2D electron gas) and electrons can then flow from one electrode to the other without strong energy barrier to overcome. A similar channel exists for holes (2D hole gas, 2DHG), which explains the much larger conductance obtained in the P/n heterostructure compared to that of the sample with a-Si:H on glass.

In order to normalize the conductance with respect to the geometry of the electrodes, one can define sheet conductance,

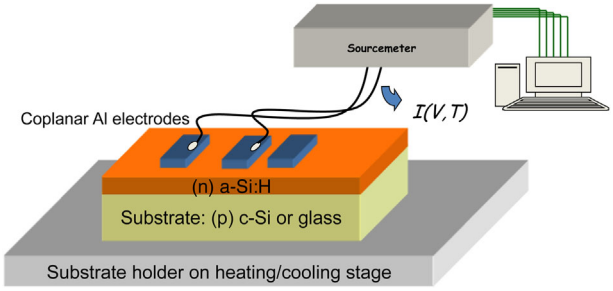

Figure 3. Measurement principle of the planar lateral conductance.

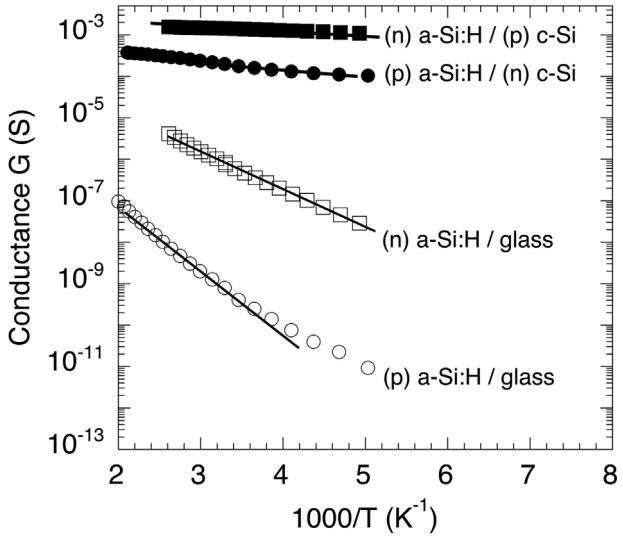

Figure 4. Arrhenius plots of the lateral conductance measured on samples of (n) a-Si:H and (p) a-Si:H deposited onto (p) c-Si and (n) c-Si wafers, respectively, or onto glass. Lines are linear fits to extract activation energies around room temperature.

$$G_S = G \times (L/h) \tag{1}$$

The sheet conductance is proportional to the sheet carrier density in the 2D gas, for example, the sheet electron density N_S in the 2DEG in the N/p heterostructure,

$$G_S = q\mu_n N_s \tag{2}$$

or sheet hole density P_S in the 2DHG in the P/n heterostructure:

$$G_S = q\mu_p P_s, \tag{3}$$

where q is the unit charge and μ_n (μ_p) is the electron (hole) mobility. The sheet electron density in the 2DEG of the N/p heterostructure is related to the integral of the electron concentration $n(x)$, x being the distance from the heterointerface:

$$N_S = \int_0^{d_{c-Si}} n(x)dx \tag{4}$$

and $d_{c\text{-}Si}$ being the thickness of c-Si. Similarly, the sheet hole density in the 2DHG of the P/n heterostructure is related to the integral of the hole concentration $p(x)$:

$$P_S = \int_0^{d_{c-Si}} p(x)dx \tag{5}$$

At a given temperature, the sheet carrier density only depends on the band bending and on the doping density in c-Si. The band bending in c-Si also depends on the a-Si:H parameters through the overall charge neutrality and Poisson's equation. Moreover, the sheet carrier density is basically activated with temperature, and the activation energy basically reflects the position of the Fermi level at the interface that is, to a certain extent, pinned by a-Si:H. The most influent parameter on the position of the Fermi level at the interface and on the activation energy of the sheet carrier density is the conduction band offset between a-Si:H and c-Si.[21] This is shown in **Figure 6** for the N/p heterostructure.

This allowed us to give a good estimate of the conduction band offset by comparing the results of Figure 6 to experimental data. Indeed, from the measured conductance, one can calculate the sheet carrier density through Equation (2) for the N/p heterostructure. To this purpose, one has to use the electron mobility in c-Si and its temperature dependence. While this is well known in the bulk, it is less well clear in a 2DEG channel. This is why we used two cases for the temperature dependence of the mobility that we considered as extreme cases: either the bulk dependence, $\mu_n = 1500\ (T/300)^{-2.4}\,\mathrm{cm^2\,V^{-1}\,s^{-1}}$ (with T the temperature in kelvin) or a temperature independent value $\mu_n = 500\,\mathrm{cm^2\,V^{-1}\,s^{-1}}$. Starting from the experimentally measured temperature dependence of the conductance of the N/p heterostructure, one can then obtain two curves for the sheet electron density (**Figure 7**).

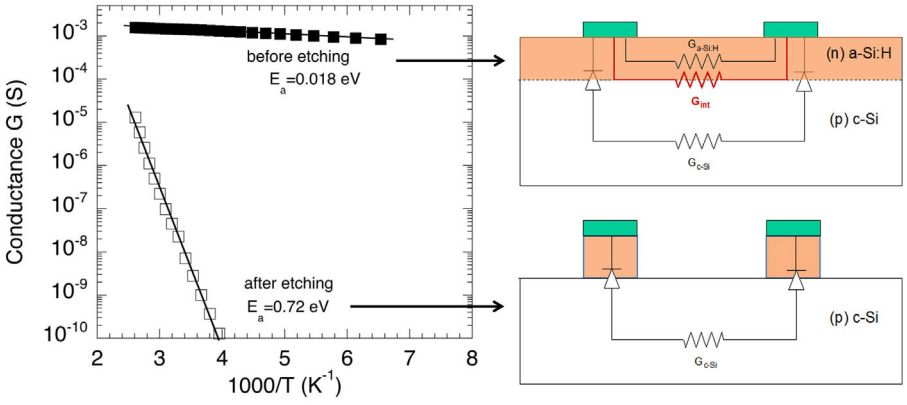

Figure 5. Arrhenius plots of the lateral conductance measured on a sample of (n) a-Si:H deposited onto (p) c-Si, before and after dry etching of the a-Si:H layers. The schematic view of the sample before and after etching also indicates a simplified electrical equivalent circuit with the various conductances corresponding to the various possible paths for current flow, and the N/p diodes. Data from Ref. [15].

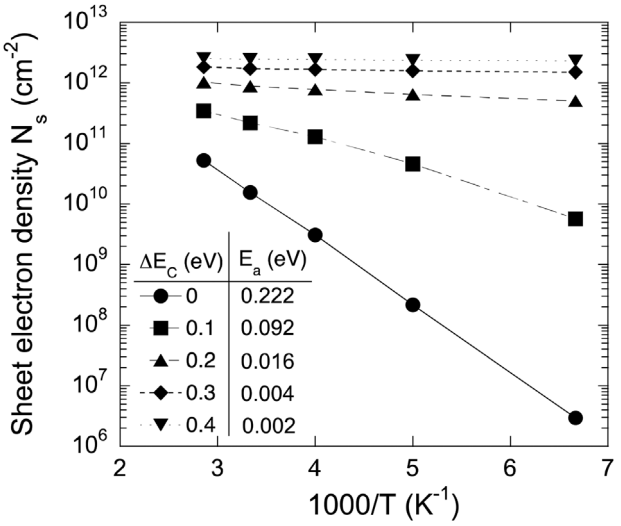

Figure 6. Arrhenius plots of the sheet electron density in c-Si calculated for various values of the conduction band offset. The insert shows the corresponding values of the activation energy determined from these plots. Data from Ref. [21].

We can extract the activation energy around room temperature corresponding to these two curves. Since the activation energy is related to the conduction band offset, these two values lead to two boundary values for the conduction band offset, as shown in **Figure 8**. This lead us to an estimate of $\Delta E_C = 0.15 \pm 0.04$ eV.[21] A deeper analysis where the influence of other a-Si:H parameters (position of the Fermi level, density of states at the Fermi level, characteristic temperature of the band tail) was taken into account, together with additional experimental data, which resulted in a slightly larger estimate of $\Delta E_C = 0.18 \pm 0.05$ eV.[22] The effect of interface states was also considered. It was shown that they could only have a significant impact on the band bending for values of the interface states density larger than $10^{12}\,cm^{-2}$.[22]

Similarly, the conductance of P/n heterostructures was shown to be very sensitive to the valence band offset. From measurements performed on a significant number of samples and from a statistical analysis, the valence band offset was estimated at $\Delta E_V = 0.36 \pm 0.04$ eV.[18] The possible effect of quantum confinement in the 2DHG was also taken into account and it was shown that it does not significantly change the extracted values of band offset.[18]

2.2. Conductive Atomic-Force Microscopy (CP-AFM)

Conductive and Kelvin probe atomic force microscopy (CP-AFM and KP-FM) techniques have proven to be powerful tools for carrier/dopant and junction profiling which are currently engineered in microelectronics.[23,24] In a natural way the capabilities of these techniques have also gained the interest of the photovoltaic community in particular to analyze material, interfaces, and junction properties.[25–27]

In this study, the properties of the a-Si:H/c-Si interface were investigated by CP-AFM using a Nanoscope IIIa Multimode AFM with the homemade electrical extension named Resiscope.[28] This extension is used in contact mode and applies a stable DC bias voltage to the device. It allows one to simultaneously measure the surface topography and the local current flowing through the AFM tip. For this purpose a conductive diamond coated AFM tip (CDT-FMR) was used, the applied force being in the range 100–500 nN. **Figure 9** schematizes the studied sample with the CP-AFM setup. The sample has a symmetric configuration where the same a-Si:H layer was deposited first on both sides of the c-Si wafer followed by ITO, the sample was thereafter cleaved before measurements.

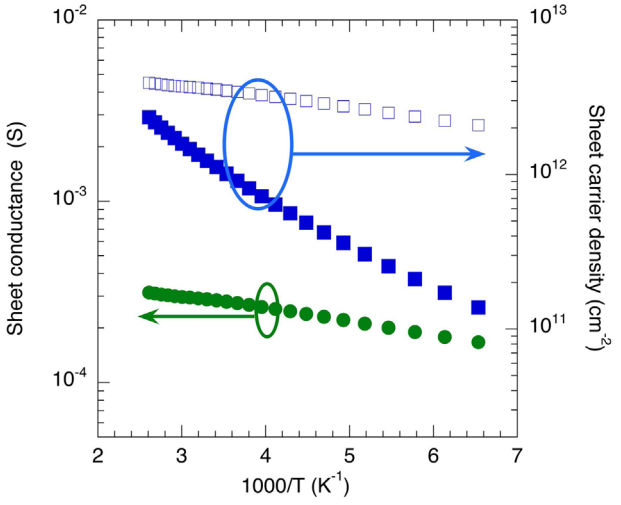

Figure 7. Arrhenius plots of the experimental sheet conductance (dots, left axis) and of the corresponding sheet carrier density calculated for two different temperature dependences of the electron mobility in c-Si: $\mu_n = 500\,cm^2\,V^{-1}\,s^{-1}$ independent of T (open squares, right axis) and $\mu_n = 1500\ (T/300)^{-2.4}\,cm^2\,V^{-1}\,s^{-1}$ (full squares, right axis).

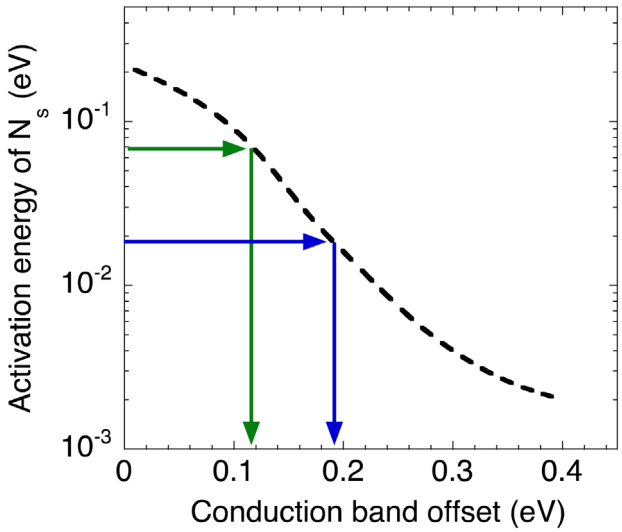

Figure 8. Dependence of the activation energy of the sheet electron density in c-Si for the N/p heterojunction as a function of the conduction band offset, ΔE_C between a-Si:H and c-Si. Data from Ref. [21].

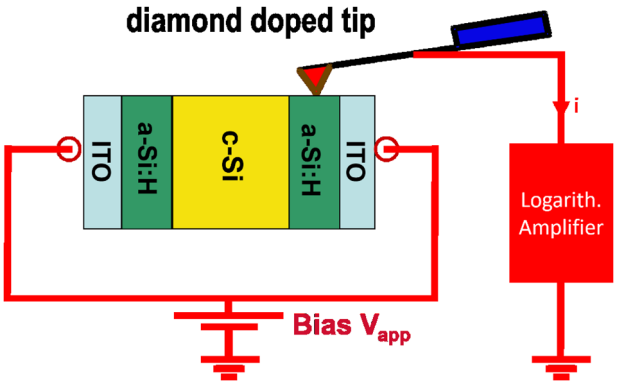

Figure 9. Sketch of the sample configuration under DC bias during the CP-AFM measurement. Both (n) a Si:H/(p) c Si/(n) a Si:H and (p) a Si:H/(n) c Si/(p) a Si:H were probed.[29] The c-Si wafer thickness was about 200 µm, while the a-Si:H thickness was 300 nm thick, deliberately thicker than in solar cells. Results in Figure 10 and 11 are shown for (n) a Si:H/(p) c Si/(n) a Si:H structures.

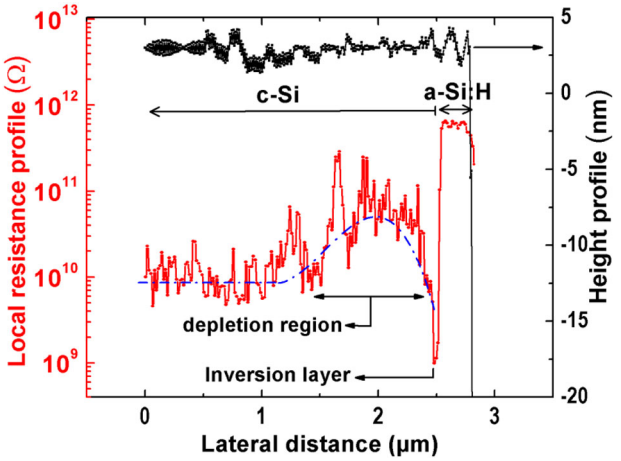

Figure 11. Local resistance (left ordinates) and height (right ordinates) profiles across the (n) a Si:H/(p) c-Si interface. Data from Ref. [29].

The thickness of the a-Si:H was deliberately chosen thick (≈300 nm) to facilitate the identification of the interface. Several pieces of cleaved samples were analysed pointing out the disruptive effects of the oxidation process taking place after cleaving or during the CP-AFM scan due to the presence of the well-known water meniscus between the tip and the surface. The optimized measurement conditions were found after a de-oxidation of the cross-section surface by an HF 1% dip and performing the AFM scans under a nitrogen atmosphere.[29] Both (n) a-Si:H/(p) c-Si and (n) a-Si:H/(p) c-Si have been probed, we here report results obtained on (n) a-Si:H/(p) c-Si samples.

Figure 10 illustrates the topography and the local resistance mapping on the cross-section after an HF dip and for an applied voltage of 1 V. The scanned area shows, from top to bottom, the n-type a-Si:H layer (≈300 nm) and the p-type c-Si substrate. The ITO contact is not observable here since it has been partially removed from the top edge with the HF treatment.

The electrical image clearly reveals a much lower resistance at the interface between the a-Si:H and the c-Si substrate. More precisely, this conductive channel is located within the c-Si substrate. Cross-sectional profiles are illustrated in **Figure 11**, where the height and local resistance values were obtained from the average of a number of AFM profiles (performed over a horizontal width of 0.5 µm in Figure 10). The profiles along the heterointerface show a flat cleavage surface (topographical variations lower than 5 nm) and a high electrical contrast between the conductive channel (<100 nm) and both the a-Si:H layer and the c-Si substrate. In addition to the conductive channel in the c-Si side it is also possible to identify a region with a decreasing conductivity of about 1 micron in width. This is the order of magnitude of the width for a depleted space charge region in c-Si. Due to the low surface roughness of the cross-section it remains important to note that the observed conductive layer cannot result from an experimental artefact. The same CP-AFM observations were also evidenced on other samples with different thicknesses of a-Si:H.[29]

The CP-AFM analysis clearly reveals a more conductive layer between the c-Si substrate and the a-Si:H film, which corresponds to the predicted strong inversion layer in (n or p) a-Si:H/ (p or n) c-Si heterojunctions (see also Figure 1 and 2).[15] However, the quantitative results of the inversion layer conductivity extracted from CP-AFM measurements have to be considered carefully. Indeed, the reliability of the latter is affected by the quality and nature of the contact between the conductive AFM tip and the sample surface. In addition, the sample surface roughness, the AFM tip radius, shape, and pressure are well-known factors driving the local electrical

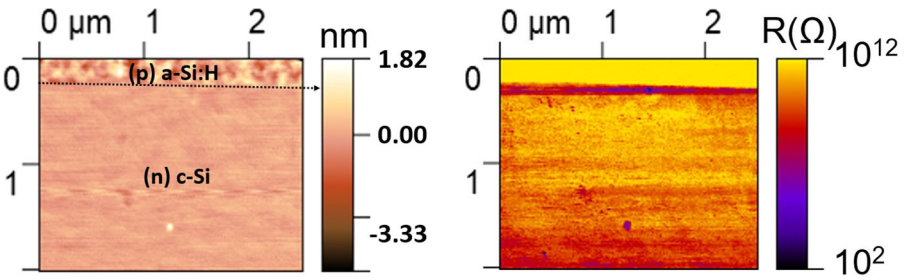

Figure 10. CP-AFM image of a cleaved section of an (n) a-Si:H/(p) c-Si heterojunction. Left: topography; right: resistance image (logarithmic scale) measured after HF dip. Data from Ref. [29].

measurements. Surface states can also induce additional band bending at the tip-surface junction modifying significantly the conductance values. Many of these limiting points have been mitigated here, thanks in particular to the HF treatment applied after cleaving which enabled to remove the native oxide on the c-Si and at the same time to temporarily passivate it.[30] The very low roughness of the surface cross-section and the nitrogen atmosphere while measuring were very beneficial in providing experimental evidence of the strong inversion layer in crystalline silicon heterojunctions.

2.3. Capacitance Measurements

Capacitance techniques are used to get insight into doping and defect properties in semiconductors. It was proposed that capacitance measurements could be used to determine band offsets in heterojunctions. Indeed, the space charge layer capacitance of a heterojunction depends on the doping density in the semiconductors and on the diffusion potential. In the depletion approximation and for uniform doping densities, the inverse square capacitance should vary linearly with the applied voltage. For instance, in an abrupt pn heterojunction between two semiconductors having permittivities ε_1 and ε_2 and doping densities N_{a1} (acceptor density of the p side) and N_{d2} (donor density of the n side):[31]

$$\frac{1}{C^2} = \frac{2}{q}\frac{(\varepsilon_1 N_{a1} + \varepsilon_2 N_{d2})(V_d - V_{app})}{(\varepsilon_1 \varepsilon_2 N_{a1} N_{d2})} \tag{6}$$

where C is the capacitance per unit area, V_d is the total diffusion voltage and V_{app} the applied voltage (in a refined analysis V_d should be replaced by $V_d - 2\ k_B T/q$, but this will be neglected in the following). Thus, the extrapolation of the linear dependence of $1/C^2$ to the voltage axis yields an intercept voltage value V_{int} that should be equal to V_d. Then, for the case of the N/p heterojunction, according to the band diagram of Figure 1, one could deduce the conduction band offset from

$$\Delta E_C = \delta^{a-Si:H} + \delta^{c-Si} - E_g^{c-Si} + qV_d \tag{7}$$

since $\delta^{c\text{-}Si}$ is known from the doping density of the wafer and $\delta^{a\text{-}Si:H}$ can be measured from the coplanar conductance technique for a-Si:H deposited on glass. Similarly, for the case of the P/n heterojunction, according to the band diagram of Figure 2, one could deduce the valence band offset from

$$\Delta E_V = \delta^{a-Si:H} + \delta^{c-Si} - E_g^{c-Si} + qV_d \tag{8}$$

Such determination of band offsets from the C-V technique has been proposed and used for III–V compounds.[32] However, for the a-Si:H/c-Si heterojunction, two major issues have to be considered: i) in a-Si:H the space charge density is not determined by the doping concentration but by the density of localized states at and close to the Fermi level; ii) depending on the measurement frequency, there might be a response of localized states due to capture and emission processes. The consequence on the C–V curve has been discussed in detail elsewhere.[33] It turns out that, due to the large DOS at the Fermi level in doped a-Si:H (whatever n- or p-type) and at moderate doping of the c-Si wafer (as it is the case in solar cell applications), the extent of the space charge layer in a-Si:H is much smaller than in c-Si. Thus P/n or N/p a-Si:H/c-Si heterojunctions behave like one-sided abrupt p+/n or n+/p junctions, respectively. At low frequency the $1/C^2$ curve follows a linear dependence as predicted by depletion layer capacitance of a one-sided abrupt junction:

$$\frac{1}{C^2} = \frac{2}{q\varepsilon N_{dop}}(V_{int} - V_{app}) \tag{9}$$

ε and N_{dop} being the permittivity and the doping density in c-Si, respectively. Examples are shown in **Figure 12** for both N/p and P/n heterojunctions. In both cases the slope of the curve yields the expected doping density of the c-Si wafer ($N_a \approx 7.5 \times 10^{14}$ cm^{-3} for the N/p structure, and $N_d \approx 1.5 \times 10^{15}\ \mathrm{cm}^{-3}$ for the P/n structure). However, if one uses the intercept voltage as the value of the diffusion potential in Equation (7) or (8), and considering the values of $\delta^{c\text{-}Si}$ and $\delta^{a\text{-}Si:H}$ that are either known from the doping of c-Si or extracted from the activation energy of the planar conductance of a-Si:H deposited on glass, one gets much lower values of band offsets than found from the lateral planar conductance analysis. For the N/p heterojunction, $\delta^{c\text{-}Si} \approx 0.25$ eV, $\delta^{a\text{-}Si:H} \approx 0.2$ eV, and $V_{int} \approx 0.65$ V, so that Equation (7) yields a value $\Delta E_C \approx 0.03$ eV if one assumes that $V_d = V_{int} + 2\ k_B T/q$, which is significantly lower than the estimate of $\Delta E_C = 0.18 \pm 0.05$ eV from the coplanar lateral conductance analysis. For the P/n heterojunction, $\delta^{c\text{-}Si} \approx 0.25$ eV, $\delta^{a\text{-}Si:H} \approx 0.35$ eV, and $V_{int} \approx 0.55$ V, so that Equation (8) yields a value $\Delta E_V \approx 0.08$ eV, which is even more significantly lower than the estimate of $\Delta E_V = 0.36 \pm 0.04$ eV from the coplanar lateral conductance analysis.

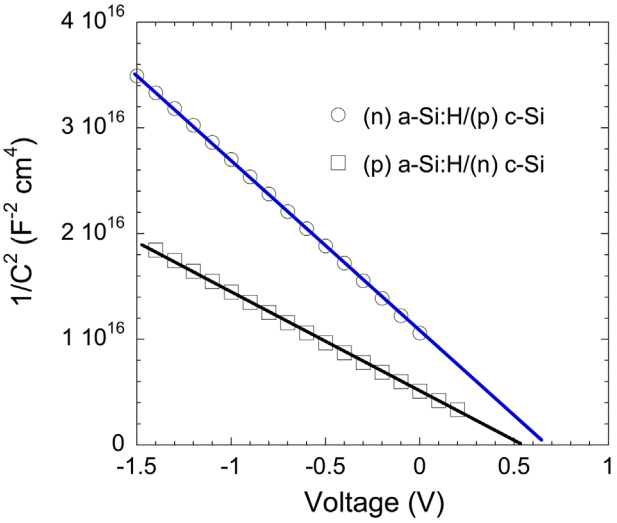

Figure 12. Voltage dependence of the inverse square capacitance (per unit area) measured on both types of heterojunctions, (n) a-Si:H/(p) c-Si and (p) a-Si:H/(n) c-Si. Full lines are linear fits to the experimental data. In each case, the slope yields the correct doping density N_{dop} that corresponds to the acceptor or donor density in c-Si, respectively.

The lower band offsets obtained from the *C–V* technique with the use of Equation (7) or Equation (8) have been explained by the presence of the strong inversion layer at the c-Si surface.[34] Indeed, it has been shown that, when a strong inversion region exists at the c-Si surface, the capacitance reflects only the depleted part of the space charge region. Therefore the value of V_{int} extracted from Equation (9) does not correspond to the total diffusion potential but only to the potential drop in the depleted part of the space charge in c-Si, or, in other words, to the band bending, ψ_{inv}, corresponding to strong inversion. An approximate expression based on the definition that the minority carrier concentration at the limit of strong inversion should be equal to the majority carrier concentration in the bulk is[35]

$$\psi_{inv} = \frac{2k_BT}{q}\ln\left(\frac{N_{dop}}{n_i}\right) \tag{10}$$

Another approximate expression has been proposed by Lindner[36] as

$$\psi_{inv} = \frac{k_BT}{q}\left[2.1\ln\left(\frac{N_{dop}}{n_i}\right) + 2.08\right] \tag{11}$$

For given values of $\delta^{c\text{-}Si}$ and $\delta^{a\text{-}Si:H}$, Equation (7) predicts that the diffusion potential should increase linearly with the conduction band offset in the N/p heterojunction (and similarly for the valence band offset using Equation (8) in the P/n heterojunction). However, above a given value of band offset the strong inversion region appears and the intercept voltage then saturates at a value which is found to be between the approximate expressions of ψ_{inv} given by Equation (10) and (11). This can be seen in **Figure 13** where V_d, V_d^{c-Si} and V_{int} were calculated for a N/p heterojunction at 300 K using a constant DOS of $10^{19}\,cm^{-3}\,eV^{-1}$ in a-Si:H and a doping density $N_a = 10^{15}\,cm^{-3}$ in c-Si. For $\delta^{a\text{-}Si:H} = 0.4$ eV, which would correspond to moderately doped (n) a-Si:H, we observe that V_d, V_d^{c-Si} and V_{int} are almost identical and increase linearly with ΔE_C up to a value of 0.2 eV. This corresponds to the situation where no strong inversion exists, the junction behaves like an n+/p junction, the potential drop in a-Si:H is negligible, the depletion approximation works well in c-Si and V_{int} is almost equal to $V_d - 2k_BT/q$ as predicted by the depletion layer theory. For $\Delta E_C > 0.2$ eV, the silicon surface becomes strongly inverted, the potential drop in a-Si:H becomes non negligible so that V_d^{c-Si} departs from V_d, and V_{int} saturates at a value corresponding to ψ_{inv}. For $\delta^{a\text{-}Si:H} = 0.2$ eV, which better corresponds to highly doped (n) a-Si:H, as found experimentally from planar conductance measurements, the total diffusion potential is increased by 0.2 eV compared to the case where $\delta^{a\text{-}Si:H} = 0.4$ eV because this corresponds to a lower work function in a-Si:H by 0.2 eV. Strong inversion along with the saturation of V_{int} then also appears for a lower value of ΔE_C by 0.2 eV (≈0 instead of ≈0.2 eV). Note that the saturation value is the same as before since it only depends on the c-Si doping which has been kept constant, and it corresponds to the value obtained experimentally on (p) type c-Si with similar doping (Figure 12). Using a more realistic DOS in a-Si:H (made of two exponential band tails and deep defect distributions) does not change the dependence on ΔE_C nor the saturated value of V_{int}, and the influence of

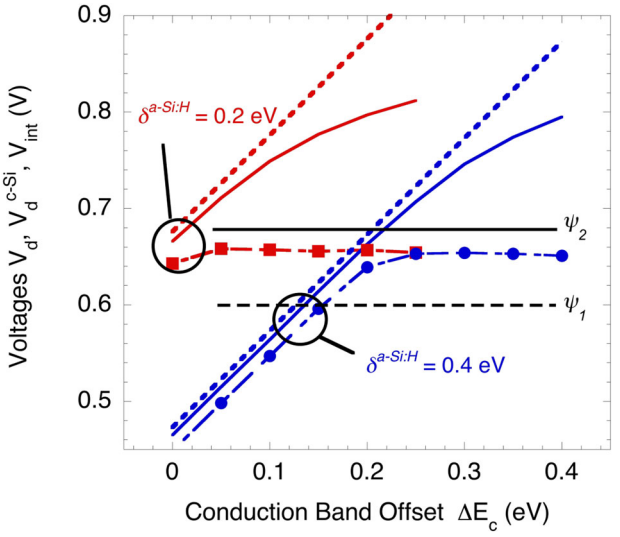

Figure 13. Calculated total diffusion voltage Vd (dashed lines), diffusion voltage in c-Si V_d^{c-Si} (plain lines) and intercept voltage of the linear fit of $1/C^2$ (symbols) for an N/p heterojunction, for two Fermi level positions in the bandgap of (n) a-Si:H, $\delta^{a\text{-}Si:H} = 0.2$ and 0.4 eV, as a function of the conduction band offset. The horizontal dashed and plain lines indicate the strong inversion band bending approximations from Equation (10) and Equation (11), respectively.

interface defects was found to be significant only for densities above $10^{12}\,cm^{-2}$.[34] In conclusion, the *C–V* technique fails to extract the correct band offset value due to the presence of the strong inversion layer, however, the value of V_{int} can indicate the presence of such a layer by comparing it to the value of ψ_{inv} calculated from Equation (10) or (11).

Finally, the presence of a strong inversion at the c-Si surface could also be emphasized from the temperature dependence of the capacitance. Indeed, it was found that the capacitance of both P/n and N/p heterojunctions increases with temperature more rapidly than predicted from the depletion layer approximation.[37] A comprehensive study of the capacitance was presented,[38] and a full modeling was developed, based on analytical and numerical calculations, where the influences of the thickness and DOS in the doped a-Si:H, as well as that of introducing a very thin undoped a-Si:H buffer layer has been studied.[39] In order to make the link with the voltage dependence, one can consider the effective diffusion voltage:

$$V_d^{eff} = \frac{q\varepsilon N_{dop}}{2C^2} \tag{12}$$

In the depletion approximation, V_d^{eff} should be equal to V_d at zero applied bias, as obtained from Equation (9). The temperature dependence should then be principally related to the shift of the Fermi level with temperature in c-Si, since the shift of the Fermi level in a-Si:H is much smaller. However, the temperature dependence obtained in the depletion approximation is much weaker than observed experimentally. This is shown in **Figure 14** for the P/n heterojunction. On the contrary, the full calculation of the capacitance, including the contribution of holes in c-Si, that become majority carriers in the strong

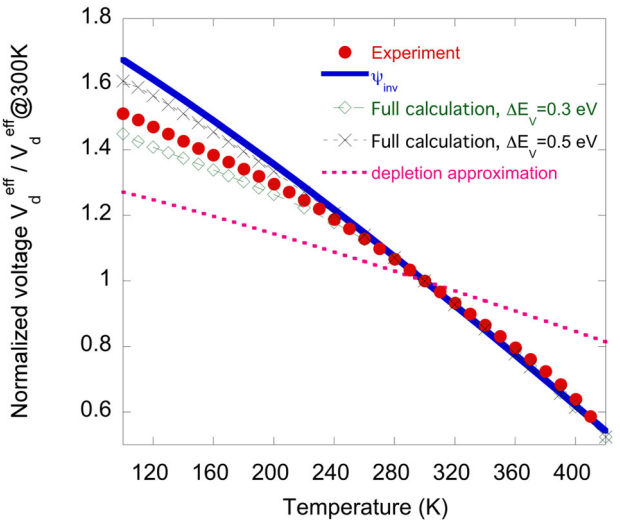

Figure 14. Effective diffusion voltage at zero DC bias, V_d^{eff}, as a function of temperature, in a P/n heterojunction. Experimental data (full dots) are compared to the band bending at the strong inversion limit, ψ_{inv}, from Equation (10) (full line) and to the values obtained from the calculation using the depletion approximation (dotted lines) or from a full calculation including the contribution of carriers in the strong inversion layer for two values of valence band offset, $\Delta E_V = 0.3$ eV (open diamonds) and $\Delta E_V = 0.5$ eV (crosses). All data have been normalized to their values at 300 K. Data from Ref. [37].

inversion layer at the c-Si surface, is able to better reproduce this stronger temperature dependence. One can see that calculations assuming a valence band offset of 0.3 and 0.5 eV nicely fit the experimental data above 250 K. Below 250 K, these are framed by the two calculated curves, which gives an estimate of the valence band offset in good agreement with that obtained from the lateral planar conductance measurements. One can also observe that the curve calculated with $\Delta E_V = 0.5$ eV is very close to that calculated with the simple expression of Equation (10). The reason is that, for such a large value of the valence band offset (all other parameters being kept constant), strong inversion almost exists at any temperature. When ΔE_V is decreased, strong inversion progressively disappears at low temperature, which creates a weaker temperature dependence, as for the curve calculated in the depletion approximation. However, when the strong inversion layer is formed, the curve becomes independent of ΔE_V and is well described by Equation (10).

3. The Role of the (i) a-Si:H Buffer Layer

As mentioned in the Introduction, one major step in the fabrication of silicon heterojunctions is the insertion of a very thin undoped (i) a-Si:H buffer layer between the doped a-Si:H layer and the c-Si wafer to passivate the a-Si(H)/c-Si interface.[8] Although post-deposition treatments like post-annealing or post-hydrogenation also play a role,[40] it has been demonstrated in previous studies that the performance of silicon heterojunction solar cells depends on the (i) layer thickness.[41–43] An optimized buffer layer thickness was generally found in the range 3–8 nm. The effect of the buffer layer has been considered by several authors,[44] the main role being to reduce the defect density at the a-Si:H/c-Si interface, attributed to silicon dangling bonds (DB), and thus decrease the interface recombination.

In the defect-pool model,[45,46] the bulk DB density in a-Si:H depends on the Fermi level position which leads to a non-uniform spatial DB distribution in an a-Si:H/c-Si heterojunction due to the band bending and spatially varying Fermi level.

We have developed a software which self-consistently calculates the DOS in both doped and undoped a-Si:H layers of a Si heterojunction by using the defect-pool model. We show here that, due to the Fermi level position dependence of the a-Si:H defect density, the thin (i) a-Si:H layer underneath the doped a-Si:H film exhibits high DB density, as had been pointed out by De Wolf.[47] We used our calculation results to extrapolate the (i) a-Si:H/c-Si interface defect density. This model allowed us to explain the increase of the effective lifetime in c-Si with the (i) a-Si:H layer thickness, as observed experimentally.

3.1. Density of States Calculated in the Defect-Pool Model

3.1.1. Defect-Pool Concept

The density of gap states in a-Si:H results from a chemical equilibrium between the weak Si-Si bonds at the origin of tail states and the dangling bonds (DB) at the origin of defect states. The DB can be formed by a chemical reaction with different mechanisms according to the hydrogen contribution to the breaking of weak Si-Si bonds in the valence band tail.[45,48] The resulting DB density $D(E)$ is composed of positively, neutral, and negatively charged defects at a range of energies E with respective densities D^+, D^0, and D^-. These defects are formed with a probability described by a distribution function for potential defect sites $P(E)$, also called the defect-pool function. $P(E)$ is a Gaussian centered at the energy E_p which corresponds to the most probable energy for the DB. This principle of the defect-pool model is illustrated in **Figure 15**.

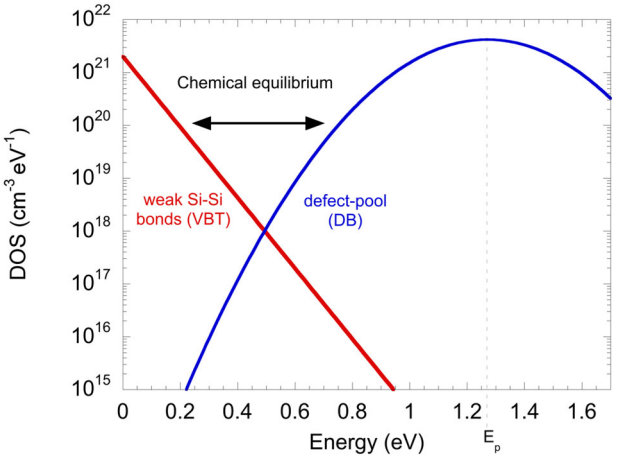

Figure 15. Scheme to illustrate the principle of the defect-pool model based on the chemical equilibrium between the weak Si-Si bonds in the valence band tail (VBT) and the dangling bonds formed with a distribution function $P(E)$ centered at E_p.

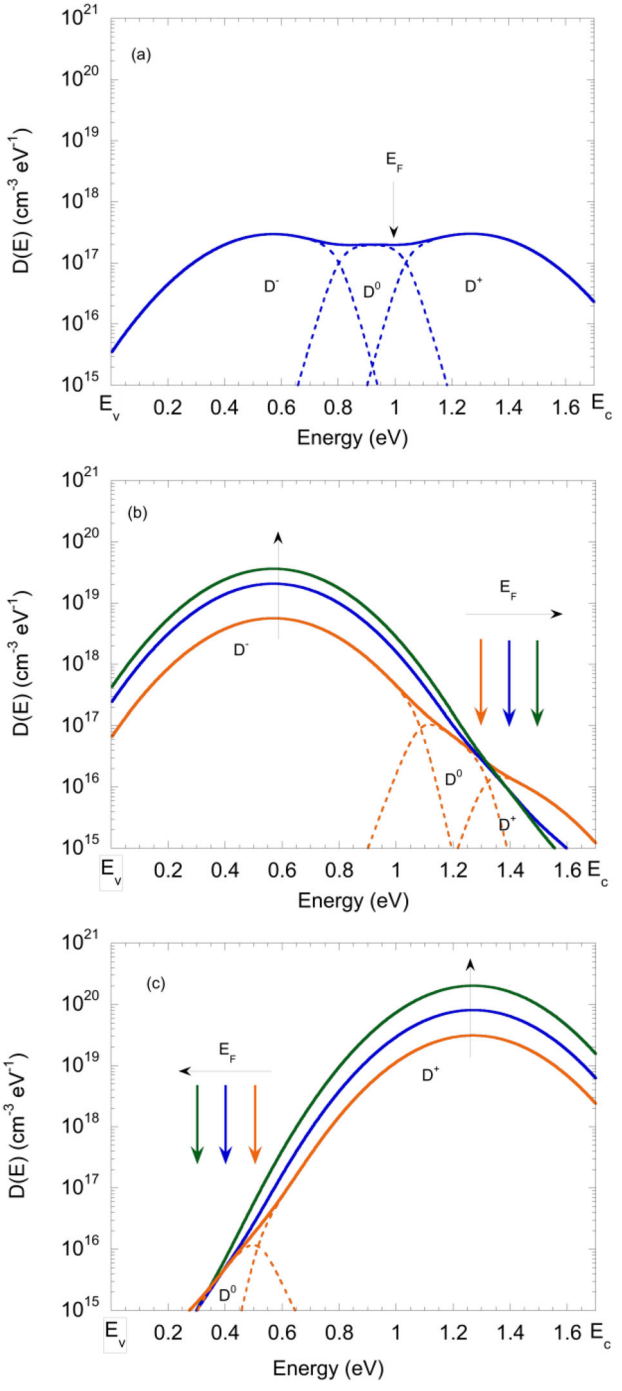

Figure 16. Calculated density of dangling bond states $D(E)$ with defect-pool parameters[46] in undoped a-Si:H (a), n-type a-Si:H (b) and p-type a-Si:H (c) at $T = 300$ K ($T_{eq} = 500$ K). In n-type (p-type) a-Si:H, the Fermi level E_F is shifted by 0.3 eV (0.5 eV)-orange, 0.4 eV (0.6 eV)-blue and 0.5 eV (0.7 eV)-green from its position in undoped a-Si:H leading to a strong increase of the D^- (D^+) density. For clarity of the figures, the D^-, D^0, and D^+ components with smaller densities are only shown for one position of the Fermi level in doped a-Si:H.

Two key elements are inherent to the defect-pool model: i) $D(E)$ is frozen in at an equilibration temperature T_{eq} (usually taken equal to 500 K)[45,49] and does not change with T as soon as T is lower than T_{eq}; ii) $D(E)$ depends on the Fermi level position and a shift of the Fermi level E_F closer to the conduction band (valence band) edge leads to an increase of the D^- (D^+) density. **Figure 16** shows the density of DB states $D(E)$ calculated with defect-pool model parameters from Powell and Deane[46] for undoped,
n-type and p-type a-Si:H and the influence of the Fermi level shift on $D(E)$.

This Fermi-level dependence is also shown on **Figure 17** where the one-electron density of states N^g is presented, integrated over energy as a function of the Fermi level position, with N^g given by

$$N^g = \int_{E_V^{a-Si:H}}^{E_C^{a-Si:H}} g(E)dE \tag{13}$$

The one-electron DOS $g(E)$ corresponds to the conversion of the DB distribution into monovalent states and is approximated by $g(E) \approx D(E + k_B T\ln(2)) + D(E - U - k_B T\ln(2))$,[46] where k_B is the Boltzmann constant and U the correlation energy taken equal to 0.2 eV in our calculation. $N^g(E)$ presents a minimum around midgap and increases exponentially as the Fermi level is shifted from midgap. Another important feature illustrated in Figure 17 is the dependence of $N^g(E)$ with the valence band tail Urbach energy E_U, which is a key parameter in the defect-pool model.

3.1.2. The Non-Homogeneous DOS in the (i) a-Si:H Layer in a Solar Cell

Studying qualitatively and quantitatively the influence of the interface defects on the (p) a-Si:H/(i) a-Si:H/(n) c-Si or (n) a-Si:H/(i) a-Si:H/(n) c-Si solar-cell performance can be complex and is usually done with the help of numerical modeling tools. In the

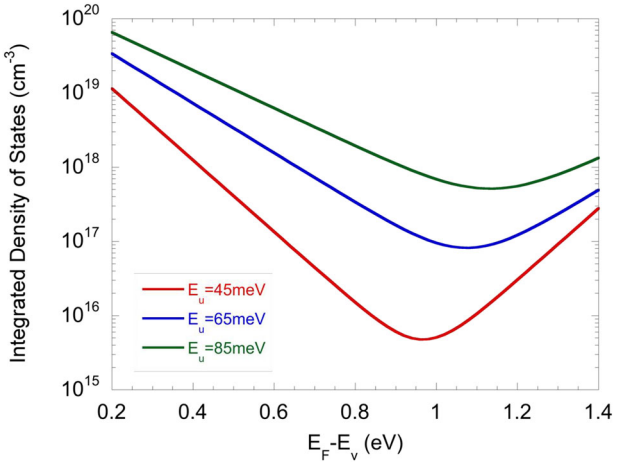

Figure 17. One-electron density of states N^g integrated over energy as a function of the Fermi level position for three values of the valence band tail Urbach energy E_u.

following, (p) a-Si:H/(i) a-Si:H/(n) c-Si and (n) a-Si:H/(i) a-Si:H/(n) c-Si structures will be written P/I/n and N/I/n, respectively.

Despite some discussions regarding spatial variation of the defect density in a-Si:H along the film growth axis due to inhomogeneities of the material,[50] and because the layers are considered thin, the density of states (exponential tails and deep defects) in both the doped and undoped a-Si:H layers is generally taken homogeneous in the whole of each layer.[51] This approximation is quite good for a thick a-Si:H layer, but band bending in a-Si:H close to the a-Si:H/c-Si interface in a heterojunction solar cell results in a non-uniform spatial DB distribution which can make this approximation inaccurate. This is precisely the case for the (i) a-Si:H buffer layer. Indeed, the defect density of the (i) a-Si:H buffer layer is usually thought to be very low but the presence of the doped a-Si:H layer imposes a Fermi level position in (i) a-Si:H much closer to the band edge (valence band edge for a P/I/n heterojunction; conduction band edge for a N/I/n heterojunction) than in a bulk undoped a-Si:H layer, leading to high DB densities. **Figure 18**a shows the DOS in a-Si:H at different points of the band diagram of a P/I/n structure: top of the (p) a-Si:H layer (pt1), (p) a-Si:H/ (i) a-Si:H interface (pt2), (i) a-Si:H/ (n) c-Si interface (pt3). The DOS in both the doped and undoped a-Si:H layers has been calculated according to the defect-pool model using a software developed in our group which self-consistently solves Poisson's equation and calculates the DB distributions.[52] We used the standard model parameters proposed by Powell and Deane,[46] except for the Urbach energy of the valence band tail that was taken equal to 86 meV in (p) a-Si:H, and 68 meV in (i) a-Si:H. The bandgap of a-Si:H and the valence band offset with c-Si were taken equal to 1.7 and 0.4 eV, respectively. We introduced an acceptor doping density in (p) a-Si:H that gives a Fermi level position $\delta^{a-Si:H} = E_F - E_V^{a-Si:H} = 0.3$ eV at pt1 (we note here that the doping density is not a good indicator for the doped a-Si:H properties, since it cannot directly reflect the free hole concentration: the Fermi level, being determined by charge neutrality, strongly depends on the DOS distribution, so the position of the Fermi level and the DOS are much better indicators). It can be observed in Figure 18b that the total density of deep defects in the (i) a-Si:H layer reaches values of 10^{19} cm^{-3} or larger, which is much higher than in thick bulk undoped a-Si:H where values are in the range 10^{15}–10^{17} cm^{-3}.[53] However, the DOS in (i) a-Si:H remains lower than in the (p) a-Si:H layer such that the defect density at the a-Si:H/c-Si interface is expected to be lower than when no buffer layer is inserted.

3.2. Surface Passivation

In light of the (i) a-Si:H buffer-layer defect properties described above, we can wonder if the defect-pool model can explain interface recombination and dependence upon (i) a-Si:H layer thickness in silicon heterojunctions. To bring answers, we have used our calculation program to determine the a-Si:H DB density profiles in an a-Si:H/c-Si heterojunction from which a surface state density D_{it} at the a-Si:H/c-Si interface has been deduced. We then studied the influence of D_{it} and of the (i) a-Si:H layer thickness on the effective carrier lifetime in symmetrical structures using the modeling software Silvaco-Atlas.[54]

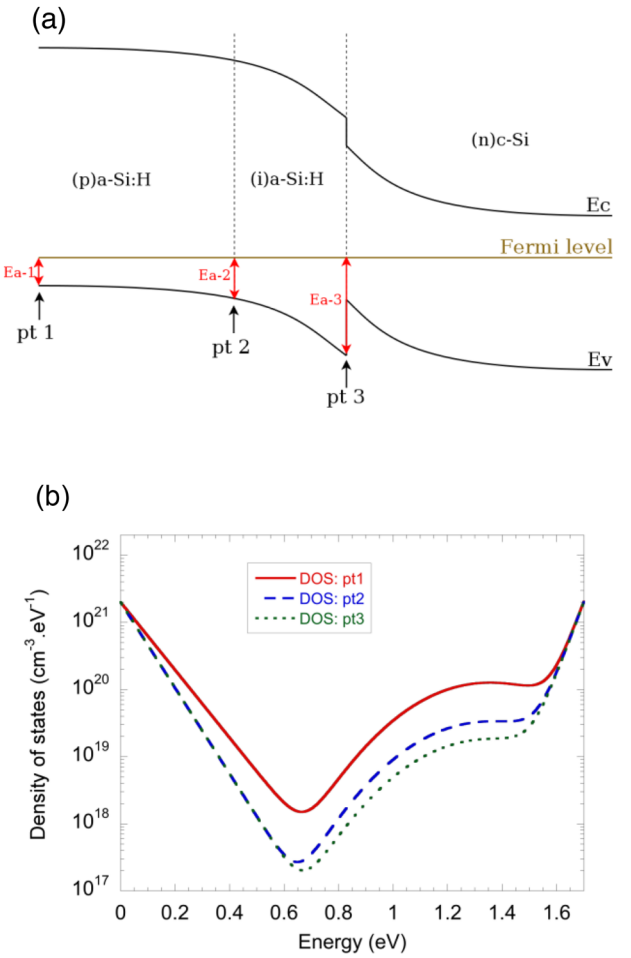

Figure 18. (a) (p) a-Si:H/(i) a-Si:H/(n) c-Si band diagram; (b) One-electron density of states in a-Si:H calculated using the defect-pool model at different points of the band diagram in (a): top of the (p) a-Si:H layer (pt 1), (p) a-Si:H/ (i) a-Si:H interface (pt 2) and (i) a-Si:H/(n) c-Si interface (pt 3). The deep defect density has been deduced from the DB distribution calculated using the defect-pool model with parameters from Powell and Deane.[46] The Urbach energy of the valence band tail has been taken equal to 86 meV in (p) a-Si:H (pt1), and 68 meV in (i) a-Si:H (pt2 and pt3). Data from Ref. [52].

3.2.1. Extrapolated Surface State Density

Recombination at the hetero-interface can be considered as volume recombination taking place in a very thin c-Si layer at the interface. Actually, c-Si wafer sawing can lead to not completely planar surfaces even after chemical cleaning, and a-Si:H and c-Si atoms bond in a disordered way on the c-Si non planar surface during the a-Si:H deposition. Thus, to model the a-Si:H/c-Si interface, we have considered a thin defective c-Si layer with a volume density of states $N_{it}(E)$. The surface defect density D_{it} is then given by

$$D_{it} = d_{int} \times \int_{E_V^{c-Si}}^{E_C^{c-Si}} N_{it}(E)dE \quad (14)$$

where d_{int} is the c-Si defective layer thickness we have taken equal to 0.5 nm.

Therefore, the first step in the extrapolation of the surface state density is to determine $N_{it}(E)$. To do so, we calculated the density of states in the doped and undoped a-Si:H layers of a silicon heterojunction using the defect-pool model. The DB distribution is then modeled by monovalent states ($g(E)$) and the total density of states $N(E)$ is the sum of the deep defect DOS ($g(E)$) and the exponential DOS of the valence and conduction band tails. $N_{it}(E)$ is obtained by the projection on the hetero-interface of the bulk states in (i) a-Si:H which are close to the interface. Since $E_g^{a-Si:H} > E_g^{c-Si}$, the projection is limited to the gap of c-Si which means that

$$N_{it}(E) = \begin{cases} 0, & E < E_V^{c-Si} \\ N(E, x=0), & E_V^{c-Si} < E < E_C^{c-Si} \\ 0, & E_C^{c-Si} < E \end{cases} \quad (15)$$

where $x = 0$ is the position of the a-Si:H/c-Si interface.

Figure 19 shows the density of monovalent states in (i) a-Si:H at the (i) a-Si:H/c-Si interface, ($N(E, x=0)$), for values of the Fermi level positions that are typical of a P/I/n heterojunction ($E_F - E_V = 0.5$ eV at the a-Si:H/c-Si interface) and an N/I/n heterojunction ($E_F - E_V = 1.45$ eV at the a-Si:H/c-Si interface). The density of states at the interface $N_{it}(E)$ is given by the restriction of $N(E, x=0)$ to the c-Si bandgap with a band offset ΔE_V taken equal to 0.4 eV.[22] Note that the model predicts larger defect density at the c-Si surface of P/I/n structures compared to N/I/n structures. This had already been discussed in terms of Fermi-level induced defect formation and Si–H bond rupture to explain better passivation properties.[47]

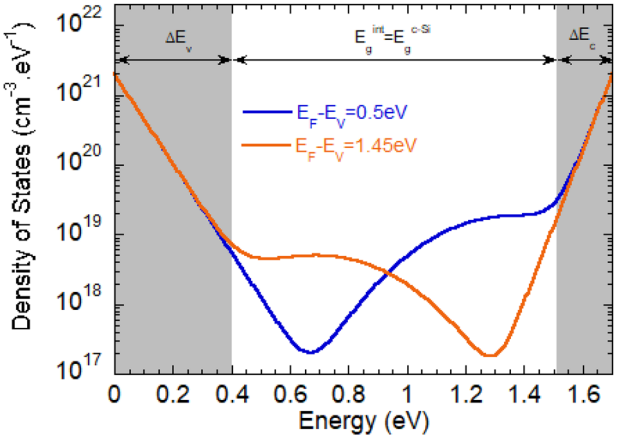

Figure 19. One-electron density of states in a-Si:H at the a-Si:H/c-Si heterointerface ($N(E)$, $x=0$) for two Fermi level positions. The deep defect density has been deduced from the DB distribution calculated using the defect-pool model with parameters from Powell and Deane[46] and the Urbach energies of the valence and conduction band tails have been taken equal to 68 and 40 meV, respectively. The density of states at the interface N_{it} is determined by restricting the distribution ($N(E)$, $x=0$) to the energy interval of the c-Si bandgap (white background).

3.2.2. Effect of the (i) a-Si:H Layer Thickness: Experimental Trends and Simulations

The effective lifetime in c-Si was measured by photoconductivity decay on symmetrical P/I/n/I/P structures with varying the (i) a-Si:H layer thickness d_i from 0 to 50 nm. The results are presented in **Figure 20**. There is a clear trend of an increasing effective lifetime with the increase of d_i.

We have compared these experimental results with simulations using Silvaco-Atlas for equivalent heterostructures with the density of monovalent states in the a-Si:H layers deduced from the defect-pool model and a surface defect density at the heterointerface calculated as described in Section 3.2.1. In all simulations, we took $E_g^{a-Si:H} = 1.7$ eV, $\Delta E_V = 0.4$ eV, and $\delta^{a-Si:H} = 0.3$ eV. More details about the simulation parameters can be found in Reaux's PhD thesis.[54]

The simulated effective lifetime results shown in **Figure 21** exhibit a different trend from the experimental measurements since the effective lifetime first increases and then decreases with d_i.

Regarding the (i) a-Si:H/(n) c-Si interface, the increase of the (i) a-Si:H layer thickness leads to an increase of the potential drop $V_d^{a-Si:H}$ and a shift of the Fermi level position closer to midgap. Thus, according to the defect-pool model, the density of states at the interface decreases (passivation by decreasing of the surface state density, so-called chemical passivation). Nevertheless, this increase of $V_d^{a-Si:H}$ also implies a decrease of the so-called field-effect passivation. Indeed, the band bending in c-Si will become weaker, meaning that the strong inversion layer at the c-Si surface, that was observed in structures without (i) a-Si:H buffer layer, gets weaker or disappears. Therefore, the concentration of minority carriers in c-Si at the a-Si:H/c-Si interface (electrons) then increases, which consequently leads to an increase of the recombination rate. For our experimental structures, the effective lifetime measurement trend shows that chemical passivation predominates over field-effect passivation

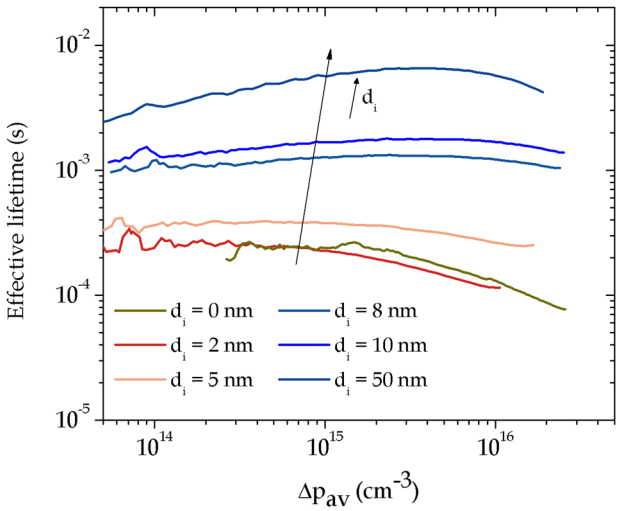

Figure 20. Effective lifetime in c-Si measured by photoconductivity decay on (p) a-Si:H/(i) a-Si:H/(n) c-Si/(i) a-Si:H/(p) a-Si:H structures with different (i) a-Si:H layer thickness d_i.

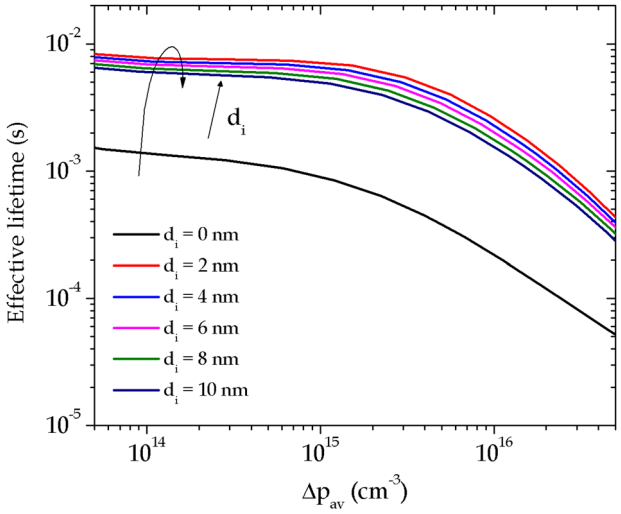

Figure 21. Simulated effective lifetime in c-Si for (p) a-Si:H/(i) a-Si:H/(n) c-Si/(i) a-Si:H/(p) a-Si:H structures equivalent to those studied experimentally.

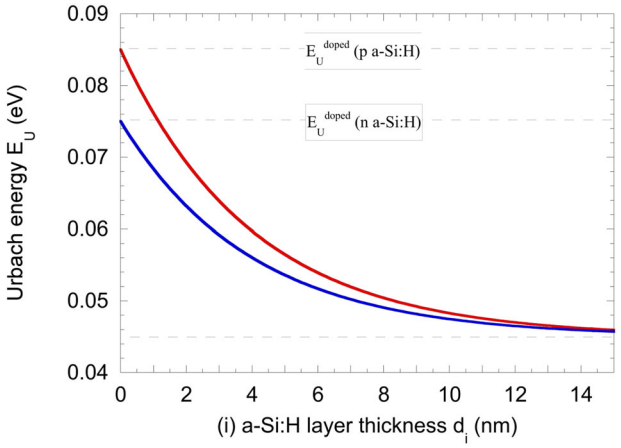

Figure 22. Exponential variation law of the Urbach energy with the (i) a-Si:H layer thickness that was integrated into our model.

as suggested by De Wolf et al.[55] In fact, the higher DB densities of a very thin (i) a-Si:H layer (a few nm) compared to thicker layers[56] can explain that a better a-Si:H/c-Si passivation quality is obtained with thicker (i) a-Si:H films. It is noted that this cannot be reproduced by our simulations, which means that the decrease of defects with the increase of (i) layer thickness calculated from the defect-pool model is not sufficient to counterbalance the decrease of the field-effect passivation. One could then argue that the defect-pool model is unable to explain the dependence of passivation quality on the (i) a-Si:H layer thickness. However, we also observed previously that the dangling bond density predicted by the model strongly depends on the Urbach energy or characteristic width of the valence bandtail. Since very thin a-Si:H layers could be more disordered than thicker layers, we implemented a thickness dependent Urbach tail in the (i) a-Si:H layer by a variation law of the Urbach energy according to

$$E_U(d_i) = E_U^{\text{doped}} + \left(E_U^{\infty} - E_U^{\text{doped}}\right) \times \left(1 - \exp\left(-\frac{d_i}{d_{\text{type}}}\right)\right) \quad (16)$$

where E_U^{∞} is the Urbach energy in a thick (i) a-Si:H layer, E_U^{doped} is the Urbach energy in the doped a-Si:H layer and d_{type} is the characteristic distance of the Urbach tail width with thickness. This variation law is represented in **Figure 22**. For $d_i = 0$ nm, the Urbach energy is taken equal to 75 meV for (n) a-Si:H and 85 meV for (p) a-Si:H and for a thick (i) a-Si:H we have chosen a value of 45 meV. These are typical values than can be found in the literature.[53,57] **Figure 23** shows the calculated effective lifetime taking into account the variation law of the Urbach energy with the buffer layer thickness. We can observe that the experimental trend with (i) layer thickness is now better reproduced. We are not aiming at producing the best fits to experimental data, however we want to indicate which parameters could be changed to make the calculated curves get closer to the experimental ones. We notice that the calculated effective lifetime values are too high compared to our experimental data (Figure 23 compared to Figure 20), which means that interface recombination is too low with the model parameters that have been taken to calculate the results of Figure 23.

There are basically two ways to increase interface recombination. The first one is to increase the interface defect density. Thus, we took larger values of Urbach energy in both doped and undoped a-Si:H layers: $E_U^{(p)a-Si:H} = 100$ meV and an exponential variation law in (i) a-Si:H with $E_U^{\infty} = 65$ meV. The electronic properties of very thin a-Si:H layers are not well known and even though these values appear quite high, they can be compatible with an increased disorder in very thin layers compared to thicker ones.[58] Calculations taking into account these larger values of Urbach energy are shown in **Figure 24**a.

Another way to increase the interface recombination is to increase the capture cross sections of the Gaussian defect distributions. It has been demonstrated elsewhere[59] that the

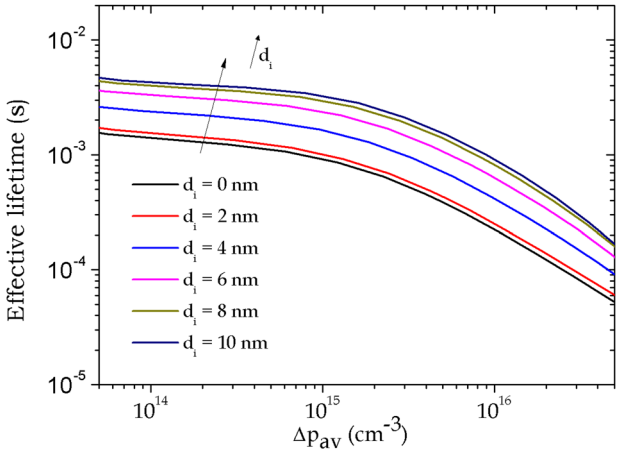

Figure 23. Simulated effective lifetime in c-Si for (p) a-Si:H/(i) a-Si:H/(n) c-Si/(i) a-Si:H/(p) a-Si:H structures equivalent to those studied experimentally taking into account the exponential variation law of the Urbach energy with thickness in the (i) a-Si:H layer.

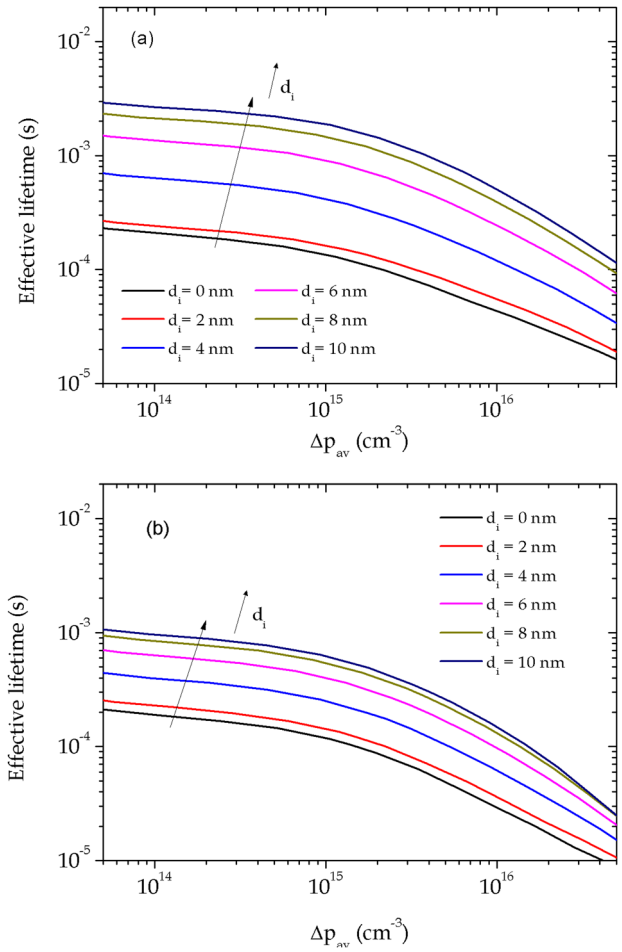

Figure 24. Simulated effective lifetime in c-Si for (p) a-Si:H/(i) a-Si:H/(n) c-Si/(i) a-Si:H/(p) a-Si:H structures equivalent to those studied experimentally taking into account the variation law of the Urbach energy given in Equation (16) with (a) $E_U^{(p)a\text{-}Si:H} = 100$ meV, $E_U^{\infty} = 65$ meV, $\sigma_n^+ = 1.3 \times 10^{-14}$ cm^2; (b) $E_U^{(p)a\text{-}Si:H} = 85$ meV, $E_U^{\infty} = 45$ meV, $\sigma_n^+ = 1.3 \times 10^{-13}$ cm^2.

capture of electrons by the donor Gaussian distribution ($D^+ + e^- \rightarrow D^0$) is dominating in the recombination process. Thus, to calculate the data shown in Figure 24b we took the same Urbach energy parameters as for Figure 23, $E_U^{(p)a-Si:H} = 85$ meV, $E_U^{\infty} = 45$ meV, thus yielding the same interface defect density, but we multiplied the capture cross section of electrons of the donor Gaussian states, σ_n^+, by a factor of ten ($\sigma_n^+ = 1.3 \times 10^{-13}$ cm^2 instead of 1.3×10^{-14} cm^2, the other capture cross sections being unchanged, $\sigma_n^0 = 2.7 \times 10^{-15}$ cm^2, $\sigma_p^0 = 8.0 \times 10^{-15}$ cm^2, $\sigma_p^- = 2.0 \times 10^{-14}$ cm^2).

Comparing Figure 24a and Figure 24b with Figure 23, we first observe that the trend of increasing effective lifetime with increasing (i) layer thickness, as observed experimentally, has not been changed because this is related to the thickness dependence of the Urbach tail parameter as proposed by Equation (16) and Figure 22. As expected, we observe that the effective lifetime values have been decreased either by increasing the Urbach energy (Figure 24a) or by increasing the electron capture cross section for positively charged dangling bonds (Figure 24b), and that they are now closer to our experimental values (Figure 20).

In conclusion of this section, the defect-pool model predicts a much higher density of dangling bond states (>10^{18} cm^{-3}) in the thin (i) a-Si:H buffer layer of a (p) a-Si:H/(i) a-Si:H/(n) c-Si or (n) a-Si:H/(i) a-Si:H/(n) c-Si structure than the usual low defect values (≈10^{16} cm^{-3}) of thick undoped a-Si:H layers. Using the defect-pool model to describe the volume deep defects in both the doped and undoped a-Si:H layers we have extrapolated the volume defect density in the (i) a-Si:H layer to the surface defect density at the a-Si:H/c-Si interface. This enabled us to reproduce the trend of experimental effective lifetime data in c-Si as a function of the (i) a-Si:H buffer layer thickness in doped a-Si:H/(i) a-Si:H/ c-Si structures. However, to do so, it was necessary to take into account a change of the width of the valence band tail in (i) a-Si:H with the buffer layer thickness. Such a change could be justified in terms of changes in the disorder in the material.

Regarding the relevance of the defect-pool model to explain passivation properties of the c-Si surface in silicon heterojunction solar cells, previous works by other groups also emphasized the asymmetry in the Fermi-level induced defect formation in P/n and N/n silicon heterojunctions,[47] or a correlation between passivation of the c-Si surface and the Urbach energy of the (i) a-Si:H layer in I/n or P/I/n structures.[60] Although the environment of dangling bonds at the interface could be different than that of bulk dangling bonds, the effects of Fermi level position and disorder (weak Si-Si bonds) seem to be mostly relevant. In some recent works, other authors obtained better surface passivation, for example, larger effective lifetimes in P/I/n structures when the (i) a-Si:H layer exhibited a larger hydrogen microstructure factor R^*.[61] This might seem to contradict results obtained from other groups, as previously mentioned. However, a larger hydrogen microstructure factor does not necessarily imply a larger Urbach energy. We have seen in our modeling that increasing the Urbach energy also increases the surface defect density, thus decreasing the effective lifetime. Similarly, decreasing the Urbach energy would produce larger effective lifetimes. One could also argue that the larger hydrogen microstructure factor could indicate changes in the local environment of dangling bonds that could decrease the capture cross section, and thus increase the effective lifetime. Moreover, hydrogen also affects the bandgap of a-Si:H. Increasing the microstructure and the bandgap of a-Si:H has not been discussed here in the frame of the defect-pool model. A shift of the pool position with increased bandgap energy could also result in a lower defect density. Such argument was for instance used to explain experimental results of better surface passivation of highly doped c-Si by a-Si:H deposited at lower temperatures, having larger bandgap.[62]

4. Concluding Remarks

The a-Si:H/c-Si heterointerface has been a matter of intensive research in the past decade. Thanks to combined experimental and modeling work, it has been possible to have a reliable picture of the band diagram at the heterojunction and to deduce values for the band offsets. Technological progress has led to outstanding device performance in solar cells with record

conversion efficiencies. This has been possible thanks to the introduction of a thin undoped a-Si:H buffer layer. The common thought is that undoped a-Si:H has a very low density of deep defects compared to doped a-Si:H, and thus leads to low interface defect density and low interface recombination for carriers generated in the c-Si absorber. Based on the defect-pool model, we have demonstrated that this common idea is not true. Indeed, due to the low band bending in the doped a-Si:H layer, the position of the Fermi level in the thin (i) a-Si:H buffer is much closer to the band edge than it would be in the bulk of thick (i) a-Si:H, leading to a much larger DOS than generally assumed. Nevertheless, increasing the (i) a-Si:H thickness screens the presence of the doped a-Si:H by increasing the potential drop in the (i) layer and shifting the Fermi level to a position closer to midgap than in the doped a-Si:H, thus inducing a reduction of the DOS at the a-Si:H/c-Si interface and therefore a reduction of the interface defect density. Simulations have shown that experimental data of effective lifetime in c-Si as a function of the (i) buffer thickness can be reproduced in the frame of the defect-pool model only if the width of the valence band tail also decreases when the (i) buffer thickness increases. This could reflect a lower density of weak Si-Si bonds and a lower degree of disorder as the (i) buffer thickness is increased, which also results in a lower deep defect density due to the equilibrium between weak bonds and deep defects. A full description of the chemistry and physics of the a-Si:H/c-Si interface (taking into account hydrogen microstructure at the interface as well as the effects of post-annealing and post-hydrogenation treatments) is not directly integrated at the moment in the defect-pool model, and we observed that some recent experimental results published in the literature regarding the link of disorder and hydrogen microstructure in the (i) a-Si:H buffer layer to c-Si surface passivation might seem contradictory. This could deserve further work in order to identify to which degree changes in the bandgap energy and pool position in the model could solve this issue. Nevertheless, the overall general idea of the model can at least provide a theoretical support to explain major experimental data and technological improvements of the a-Si:H/c-Si based solar cell properties.

Acknowledgements

We would like to thank all the people who provided many samples that have been studied (Pere Roca I Cabarrocas, Delfina Muñoz, Stefaan De Wolf, Nazir Kherani, . . .). This work would not have been possible without the contribution of several PhD students (Moussa Soro, Wilfried Favre, Renaud Varache, Olga Maslova, Tristan Carrere, David Reaux) and post-doctoral fellows (Alexander Gudovskikh).

Conflict of Interest

The authors declare no conflict of interest.

Keywords

amorphous silicon, crystalline silicon, interfaces, passivation

Received: November 14, 2018
Revised: March 27, 2019
Published online: May 16, 2019

[1] a) D. M. Chapin, C. S. Fuller, G. L. Pearson, *J. App. Phys.* **1954**, *25*, 676; b) M. A. Green, *Prog. Photovolt. Res. Appl.* **2009**, *17*, 183.
[2] a) W. E. Spear, P. G. LeComber, *Solid State Commun.* **1975**, *17*, 1193; b) E. Carlson, C. R. Wronski, *Appl. Phys. Lett.* **1976**, *28*, 671; c) D. E. Carlson, *IEEE Trans. ED* **1977**, *24*, 449.
[3] Y. Hamakawa, *Sol. Energy Mater.* **1982**, *8*, 101.
[4] a) M. V. C. Stroomer, M. J. Powell, B. C. Easton, J. A. Chapman, *Electron. Lett.* **1982**, *18*, 858; b) T. Tsukada, *Electron. Comm. Jpn.* **1994**, *77*, 38; c) J. Jang, S. H. Won, B. S. Kim, M. P. Hong, K. H. Chung, in *Flexible Flat Panel Displays* (Ed: G. P. Crawford), John Wiley & Sons Ltd., Chichester, England **2005**, Ch. 22.
[5] a) E. L. Salabaş, A. Salabaş, B. Mereu, O. Caglar, M. Kupich, J. S. Cashmore, I. Sinicco, *Prog. Photovolt: Res. Appl.* **2016**, *24*, 1068; b) H. Sai, T. Matsui, M. Koji, *Appl. Phys. Lett.* **2016**, *109*, 183506; c) M. Stuckelberger, R. Biron, N. Wyrsch, F.-J. Haug, C. Ballif, *Renewable Sustainable Energy Rev.* **2017**, *76*, 1497.
[6] *Photovoltaics Report*, Fraunhofer Institute for Solar Energy Systems, Freiburg, 27 August **2018**, http://www.ise.fraunhofer.de/de/downloads/pdf-files/aktuelles/photovoltaics-report-in-englischer-sprache.pdf, accessed Oct 2018.
[7] a) J. I. Pankove, M. L. Tarng, *Appl. Phys. Lett.* **1979**, *34*, 156; b) Y. Hamakawa, K. Fujimoto, K. Okuda, Y. Kashima, S. Nonomura, H. Okamoto, *Appl. Phys. Lett.* **1983**, *43*, 644; c) K. Okuda, H. Okamoto, Y. Hamakawa, *Jpn. J. Appl. Phys.* **1983**, *22*, L605.
[8] M. Tanaka, M. Taguchi, T. Matsuyama, T. Sawada, S. Tsuda, S. Nakano, H. Hanafusa, Y. Kuwano, *Jap. J. Appl. Phys.* **1992**, *31*, 3518.
[9] K. Yoshikawa, H. Kawasaki, W. Yoshida, T. Irie, K. Konishi, K. Nakano, T. Uto, D. Adachi, M. Kanematsu, H. Uzu, K. Yamamoto, *Nat. Energy* **2017**, *2*, 17032.
[10] a) E. Maruyama, A. Terakawa, M. Taguchi, Y. Yoshimine, D. Ide, T. Baba, M. Shima, H. Sakata, M. Tanaka, *4th World Conference on Photovoltaic Energy Conversion*, 7–12 May **2006**, Waikoloa, HI, USA, DOI: 10.1109/WCPEC.2006.279743; b) M. Taguchi, A. Terakawa, E. Maruyama, M. Tanaka, *Prog. Photovolt: Res. Appl.* **2005**, *13*, 481.
[11] S. De Wolf, A. Descoeudres, Z. C. Holman, C. Ballif, *Green* **2012**, *2*, 7.
[12] a) R. Brüggemann, S. Reynolds, *J. Non-Cryst. Solids* **2006**, *352*, 1888; b) J. A. Giesecke, M. C. Schubert, B. Michl, F. Schindler, W. Warta, *Sol. Energy Mater. Sol. Cells* **2011**, *95*, 1011; c) R. A. Sinton, A. Cuevas, *Appl. Phys. Lett.* **1996**, *69*, 2510; d) D. Macdonald, R. A. Sinton, A. Cuevas, *J. Appl. Phys.* **2001**, *89*, 2772; e) W. R. Fahrner, in *Amorphous Silicon / Crystalline Silicon Heterojunction Solar Cells*, (Ed. W. R. Fahrner), Springer-Verlag Berlin Heidelberg, **2013**.
[13] D. C. Allan, J. D. Joannopoulos, *Phys. Rev. Lett.* **1980**, *44*, 43.
[14] T. F. Schulze, L. Korte, F. Ruske, B. Rech, *Phys. Rev. B* **2011**, *83*, 165314.
[15] J. P. Kleider, Y. M. Soro, R. Chouffot, A. S. Gudovskikh, P. Roca i Cabarrocas, J. Damon-Lacoste, D. Eon, P.-J. Ribeyron, *J. Non-Cryst. Solids* **2008**, *354*, 2641.
[16] B. Halliop, M. F. Salaun, W. Favre, R. Varache, M. E. Gueunier-Farret, J. P. Kleider, N. P. Kherani, *J. Non-Cryst. Solids* **2012**, *358*, 2227.
[17] W. Favre, M. Labrune, F. Dadouche, A. S. Gudovskikh, P. Roca i Cabarrocas, J. P. Kleider, *Phys. Status Solidi C* **2010**, *7*, 1037.
[18] R. Varache, J. P. Kleider, W. Favre, L. Korte, *J. Appl. Phys.* **2012**, *112*, 123717.
[19] Y. Veschetti, J. C. Muller, J. Damon-Lacoste, P. Roca i Cabarrocas, A. S. Gudovskikh, J. P. Kleider, P. J. Ribeyron, E. Rolland, *Thin Solid Films* **2006**, *511/512*, 543.

[20] a) P. Roca i Cabarrocas, *J. Non-Cryst. Solids* **2000**, *266*, 31; b) P. Roca i Cabarrocas, N. Chaâbane, A. V. Kharchenko, S. Tchakarov, *Plasma Phys. Control. Fusion* **2004**, *46*, B235.
[21] J. P. Kleider, A. S. Gudovskikh, P. Roca i Cabarrocas, *Appl. Phys. Lett.* **2008**, *92*, 162101.
[22] R. Varache, W. Favre, L. Korte, J. P. Kleider, *J. Non-Cryst. Solids* **2012**, *358*, 2236.
[23] P. Eyben, T. Janssens, W. Vandervorst, *Mat. Sci. Eng. B Solid* **2005**, *124–125*, 45.
[24] T. Hantschel, C. Demeulemeester, P. Eyben, V. Schulz, O. Richard, H. Bender, W. Vandervorst, *Phys. Status Solidi A* **2009**, *206*, 2077.
[25] H. R. Moutinho, R. G. Dhere, C.-S. Jiang, T. Gessert, A. Duda, M. Young, W. K. Metzger, M. M. Al-Jassim, *J. Vac. Sci. Technol. B* **2007**, *25*, 361.
[26] J. Kim, S. Yeon Kim, C.-S. Jiang, K. Ramanathan, M. M. Al-Jassim, *Appl. Phys. Lett* **2014**, *104*, 063902.
[27] P. Narchi, J. Alvarez, P. Chrétien, G. Picardi, R. Cariou, M. Foldyna, P. Prod'homme, J.-P. Kleider, P. Roca i Cabarrocas, *Nanoscale Res. Lett.* **2016**, *11*, 55.
[28] F. Houze, O. Schneegans, L. Boyer, *Appl. Phys. Lett.* **1996**, *13*, 1975.
[29] J. P. Kleider, J. Alvarez, A. V. Ankudinov, A. S. Gudovskikh, E. V. Gushina, M. Labrune, O. Maslova, W. Favre, M. E. Farret-Gueunier, P. Roca i Cabarrocas, E. I. Terukov, *Nanoscale Res. Lett.* **2011**, *6*, 152.
[30] A. Danel, F. Souche, T. Nolan, Y. Le Tiec, P. J. Ribeyron, *Solid State Phenom.* **2012**, *187*, 345.
[31] S. M. Sze, *Physics of Semiconductor Devices*, 2nd edition, John Wiley & Sons, New York, USA **1981**.
[32] S. R. Forrest, in *Heterojunction Band Discontinuities – Physics and Device Applications* (Eds: F. Capasso, G. Margaritondo), North-Holland, Amsterdam **1987**, Ch. 8.
[33] J. P. Kleider, in *Physics and Technology of Amorphous-Crystalline Heterostructure Silicon Solar Cells* (Eds: W. G. J. H. M. van Sark, L. Korte, F. Roca), Springer-Verlag, Berlin Heidelberg, **2012**, Ch. 12.
[34] A. S. Gudovskikh, S. Ibrahim, J.-P. Kleider, J. Damon-Lacoste, P. Roca i Cabarrocas, Y. Veschetti, P.-J. Ribeyron, *Thin Solid Films* **2007**, *515*, 7481.
[35] E. H. Nicollian, J. R. Brews, *MOS (Metal Oxyde Semiconductor) Physics and Technology*. John Wiley & Sons, New York, USA **1982**.
[36] R. Lindner, *Bell Syst. Tech. J.* **1962**, *41*, 803.
[37] O. Maslova, A. Brézard-Oudot, M. E. Gueunier-Farret, J. Alvarez, W. Favre, D. Muñoz, J. P. Kleider, *Appl. Phys. Lett.* **2013**, *103*, 183907.
[38] J.-P. Kleider, J. Alvarez, A. Brézard-Oudot, M.-E. Gueunier-Farret, O. Maslova, *Sol. Energy Mater. Sol. Cells* **2015**, *135*, 8.
[39] O. Maslova, A. Brézard-Oudot, M.-E. Gueunier-Farret, J. Alvarez, J.-P. Kleider, *J. Appl. Phys.* **2015**, *118*, 114507.
[40] a) S. De Wolf, M. Kondo, *J. Appl. Phys.* **2009**, *105*, 103707; b) A. Descoeudres, L. Barraud, S. De Wolf, B. Strahm, D. Lachenal, C. Guérin, Z. C. Holman, F. Zicarelli, B. Demaurex, J. Seif, J. Holovsky, C. Ballif, *Appl. Phys. Lett.* **2011**, *99*, 123506; c) J. Shi, M. Boccard, Z. Holman, *Appl. Phys. Lett.* **2016**, *109*, 031601.
[41] N. Dwivedi, S. Kumar, A. Bisht, K. Patel, S. Sudhakar, *Sol. Energy* **2013**, *88*, 31.
[42] a) Y. Hayashi, D. Li, A. Ogura, Y. Ohshita, *IEEE J. Photovoltaics* **2013**, *3*, 1149; b) M. Lu, U. Das, S. Bowden, S. Hegedus, R Birkmire, *Proceedings of the 34th IEEE Photovoltaic Specialists Conference*, Philadelphia, PA (USA), June **2009**, 001475.
[43] D. Muñoz, T. Desrues, P. J. Ribeyron, in *Physics and Technology of Amorphous Crystalline Heterostructure Silicon Solar Cells* (Eds: W. G. J. H. M. van Sark, L. Korte, F. Roca), Springer-Verlag, Berlin Heidelberg, **2012**, Ch. 17.
[44] M. Ghannam, G. Shehadah, Y. Abdulraheem, J. Poortmans, *Sol. Energy Mater. Sol. Cells* **2015**, *132*, 320.
[45] M. J. Powell, S. C. Deane, *Phys. Rev. B* **1993**, *48*, 10815.
[46] M. J. Powell, S. C. Deane, *Phys. Rev. B* **1996**, *53*, 10121.
[47] S. De Wolf, in *Physics and Technology of Amorphous Crystalline Heterostructure Silicon Solar Cells* (Eds: W. G. J. H. M. van Sark, L. Korte, F. Roca), Springer-Verlag, Berlin Heidelberg, **2012**, Ch. 7.
[48] R. A. Street, K. Winer, *Phys. Rev. B* **1989**, *40*, 6236.
[49] K. Winer, *Phys. Rev. B* **1990**, *41*, 12150.
[50] a) H. Curtins, M. Favre, in *Amorphous Silicon and Related Materials* (Ed. Hellmut Fritzche), World Scientific Publishing Co. Pte. Ltd., Singapore, **1989**, Ch. 2; b) M. Favre, H. Curtins, A. V. Shah, *J. Non-Cryst. Solids* **1987**, *97-98*, 731; c) T. Shimizu, X. Xu, H. Kidoh, A. Morimoto, M. Kumeda, *J. Appl. Phys.* **1988**, *64*, 5045.
[51] a) F. Wang, Y. Gao, Z. Pang, L. Yang, J. Yang, *RSC Adv.* **2017**, *7*, 26776; b) A. Datta, M. Rahmouni, M. Nath, R. Boubekri, P. Roca, I Cabarrocas, P. Chatterjee, *Sol. Energy Mater. Sol. Cells* **2010**, *94*, 1457; c) S. Zhong, X. Hua, W. Shen, *IEEE Trans. Electron Devices* **2013**, *60*, 2104.
[52] D. Reaux, J. P. Kleider, M. E. Gueunier-Farret, *Proc. of the 29th European Photovoltaic Solar Energy Conference and Exhibition*, Amsterdam (The Netherlands), September **2014**, 1158.
[53] a) D. V. Lang, J. D. Cohen, J. P. Harbison, *Phys. Rev. B* **1982**, *25*, 5285; b) M. Stutzmann, D. K. Biegelsen, R. A. Street, *Phys. Rev. B* **1987**, *35*, 5666; c) M. Stutzmann, *Philos. Magazine Part B* **1989**, *60*, 531.
[54] D. Reaux, *PhD Thesis*, Université Paris-Sud, June, **2017**.
[55] S. De Wolf, S. Olibet, C. Ballif, *Appl. Phys. Lett.* **2008**, *93*, 032101.
[56] L. Korte, A. Laades, M. Schmidt, *J. Non-Cryst. Solids* **2006**, *352*, 1217.
[57] Y. Pan, F. Inam, M. Zhang, D. A. Drabold, *Phys. Rev. Lett.* **2008**, *100*, 206403.
[58] M. Schmidt, A. Schoepke, L. Korte, O. Milch, W. Fuhs, *J. Non-Cryst. Solids* **2004**, *338*, 211.
[59] D. Reaux, J. Alvarez, M. E. Gueunier-Farret, J. P. Kleider, *Energy Procedia* **2015**, *77*, 153.
[60] T. F. Schulze, C. Leendertz, N. Mingirulli, L. Korte, B. Rech, *Energy Procedia* **2011**, *8*, 282.
[61] A. Descoeudres, C. Allebé, N. Badel, L. Barraud, J. Champliaud, G. Christmann, F. Debrot, A. Faes, J. Geissbühler, J. Horzel, A. Lachowicz, J. Levrat, S. Martin de Nicolas, S. Nicolay, B. Paviet-Salomon, L.-L. Senaud, C. Ballif, M. Despeisse, *Sol. Energy* **2018**, *175*, 54.
[62] K. Carstens, M. Dahlinger, *J. Appl. Phys.* **2016**, *119*, 185303.